

Article

Evaluation of the Composite Mechanism of Nano-Fe₂O₃/Asphalt Based on Molecular Simulation and Experiments

Yuhao He ¹, Qing Zeng ^{2,3}, Yaru Liu ^{3,4,*}, Peng Liu ¹, Yuqin Zeng ², Zhenghong Xu ¹ and Qicheng Liu ^{1,2,3}

¹ School of Materials Science and Engineering, Changsha University of Science & Technology, Changsha 410114, China; heyuhao_csust@163.com (Y.H.); liupengmse@csust.edu.cn (P.L.); 13955427279@163.com (Z.X.); qichengliu1856@163.com (Q.L.)

² School of Physics & Electronic Science, Changsha University of Science & Technology, Changsha 410114, China; ZengQing@stu.csust.edu.cn (Q.Z.); zengyq1996@hotmail.com (Y.Z.)

³ Hunan Provincial Key Laboratory of Flexible Electronic Materials Genome Engineering, Changsha 410114, China

⁴ School of Traffic & Transportation Engineering, Changsha University of Science & Technology, Changsha 410114, China

* Correspondence: lyr901013@163.com

Abstract: Asphalt, as an indispensable binder in road paving, plays an important role in transportation development. However, the mechanism of action between the modifier and asphalt cannot be fully explained by the existing test methods. This paper combines molecular simulations with experiments to provide a research and analysis tool to evaluate the “structure–performance” relationship of asphalt. From the trend of experimental results, the optimal content of Nano-Fe₂O₃ is 1% to 3%. The AFM micrograph of the asphalt material shows that at 3%, the Nano-Fe₂O₃ can be effectively dispersed in the asphalt and the unique “bee structures” of the asphalt can be adsorbed around the modifier. Molecular dynamics studies and results show that when Nano-Fe₂O₃ are incorporated into the asphalt and have a strong adsorption force on the colloidal structure of asphalt, the “bee structures” can be adsorbed around the Nano-Fe₂O₃. In the range of 208–543 K, the sol-gel structure of asphalt in the Nano-Fe₂O₃/asphalt composite system is gradually disrupted.

Keywords: nano-Fe₂O₃; asphalt; AFM; molecular simulation; radial distribution function



Citation: He, Y.; Zeng, Q.; Liu, Y.; Liu, P.; Zeng, Y.; Xu, Z.; Liu, Q. Evaluation of the Composite Mechanism of Nano-Fe₂O₃/Asphalt Based on Molecular Simulation and Experiments. *Materials* **2021**, *14*, 3425. <https://doi.org/10.3390/ma14123425>

Academic Editor:
Francesco Canestrari

Received: 22 April 2021
Accepted: 17 May 2021
Published: 21 June 2021

Publisher's Note: MDPI stays neutral with regard to jurisdictional claims in published maps and institutional affiliations.



Copyright: © 2021 by the authors. Licensee MDPI, Basel, Switzerland. This article is an open access article distributed under the terms and conditions of the Creative Commons Attribution (CC BY) license (<https://creativecommons.org/licenses/by/4.0/>).

1. Introduction

In recent years, more and more researchers are using nanomaterials to improve the drawbacks arising from the use of asphalt and asphalt composites [1].

Liao [2] et al. improved the resistance to aging under UV light by incorporating Nano-TiO₂ into asphalt binders. Their results showed that the incorporation of Nano-TiO₂ had a positive effect on the aging of asphalt binders, reducing the rate of aging as well as improving the asphalt road performance [3]. They added different ratios of TiO₂ and ZnO to the asphalt binder and exposed the modified asphalt to sunlight for a long enough period of time. It has been shown that the temperature of TiO₂ and ZnO modified asphalt was on average 1.88 °C lower than that of unmodified one [4]. In both samples containing 2% and 4% nanomaterials, the free energy of adhesion of the asphalt binder was increased, which made more energy required to separate the asphalt binder from the aggregate surface [5]. A. Ābele [6] modified RTFOT with recycled polymers to show better low-temperature performance, as well as greater resistance to rutting and fatigue. The experimental results showed that the application of nanomaterials reduced the debonding energy and was thermodynamically more stable. The experimental results with different nano-modifier dosing showed that the improvement of peel resistance of asphalt mixes was more significant with nano-Fe₂O₃.

Up to now, very few studies have explored the interaction between the modifier and asphalt. Peng Wang [7] chose the SARA component structure model to study the interactions of asphaltenes, saturated fractions, aromatic fractions, and gums. The results show that van der Waals is the main force controlling the intermolecular interactions. The arrangement of SARA fractions for intermolecular interactions in asphalt is essentially consistent with modern colloid theory. Albert M. Hung [8] showed by simulations and computational analysis that the interactions between wax and asphalt components (<22 kcal/mol) are much weaker than those of the asphalt components themselves (>50 kcal/mol). With the availability of molecular simulation techniques, it is possible to bring our study of asphalt composites to a smaller scale for cross-scale studies.

With the advent of modern chromatographic techniques, Corbett [9] proposed elution-adsorption liquid chromatography of activated alumina with solvents of increasing polarity and aromaticity separate components other than asphaltenes into saturates, aromatics, and gums. As a result of this method, the composition of bitumen is usually divided into saturates, aromatics, gums, and asphaltenes, the so-called SARA fraction [10].

However, the effect of nanoparticles on the macroscopic properties of asphalt composites and their modification mechanisms are still unclear. In this work, we started from the question of whether nano-Fe₂O₃ can enhance the performance of asphalt and the uncertain mechanism of interaction between nano-Fe₂O₃ and asphalt. Molecular simulation of nano-Fe₂O₃ with asphalt using molecular dynamics aims to reveal the effect of nano-Fe₂O₃ on asphalt properties as well as to explain the interaction mechanism between nano-Fe₂O₃ and asphalt at the molecular level. It overcomes the problem of asphalt as an extremely complex mixture, and the mechanism of interaction between nano-Fe₂O₃ and asphalt is difficult to be revealed by conventional detection means. It also bridges the gap of the current research in this area and promotes the better application of molecular simulation methods in the field of asphalt.

2. Experimental and Simulation Calculation Details

2.1. Experimental Details

The 70# matrix asphalt (Hunan Baoli Asphalt Co., Ltd, Changsha, China) was placed in the oven at 130 °C for 1 h. After the matrix asphalt had certain fluidity, the matrix asphalt was placed in a beaker according to the amount required for the experiment. The beaker was placed in an oil bath and heated to 150 °C with constant stirring until the asphalt was in a molten homogenize state. Nanoscale α -Fe₂O₃ was used as the modifier. The Nano-Fe₂O₃ were added to the asphalt in different doses and homogenized with the matrix asphalt in a high homogenizer at a temperature of 150 °C at 6000 r/min for 45 min. The prepared Nano-Fe₂O₃/asphalt composites were poured into the molds required for testing and cooled to test conditions, and the rest of the composites were cooled to room temperature for subsequent testing. The nanoparticle characteristics are shown in the SEM image (Hitachi S-4800, Hitachi, Tokyo, Japan) in Figure 1. The size is about 90–150 nm.

2.2. Simulation Calculation Details

Saturated hydrocarbons are shown in Fourier transform infrared spectroscopy (FTIR) to contain different branched structures and some long aliphatic chains and small amounts of cycloalkanes with traces of polar atoms and aromatic rings. It usually represents 5 to 15 wt.% of the total asphalt [9,11,12]. Asphalt contains more than 40% to 50% of saturated aromatic hydrocarbons, and they are mostly a mixture of hydrocarbons and non-compounds. The term mixture of hydrocarbons refers to the presence of cycloalkane rings and alkyl side chains and aromatic rings in the same molecule. Gums are also known as polar aromatic hydrocarbons, with a lower structure of compound aromatic hydrocarbons. Gums usually contain two to four fused rings and are sometimes more polar than asphaltenes [13–15]. The molecular structure of asphaltenes, compared to other components in asphalt, has been the focus of research on asphaltene materials in the last decade, leading to the gradual identification of representative molecular models for

asphaltenes. Asphaltene H/C ratios range from 0.98 to 1.56 [16], and as shown by UV fluorescence [12,14], FTIR [12,14], X-ray Raman spectroscopy [17], and NMR [15,18,19], the molecular model of asphaltenes contains fused aromatic rings with a maximum value of the UV fluorescence spectrum around 450 nm [14], then the possible structures correspond to 4 to 10 aromatic rings and a certain amount of aliphatic chains. Many polar groups are also present in asphalt molecules [20], but the presence of molten aromatic structures is still a fundamental feature that distinguishes asphalt molecules from others [21]. In this paper, we use the Yen-Mullins [14,21,22] molecular model, which is characterized by the sulfur atom located in the thiophene ring and the construction of some aliphatic chains.

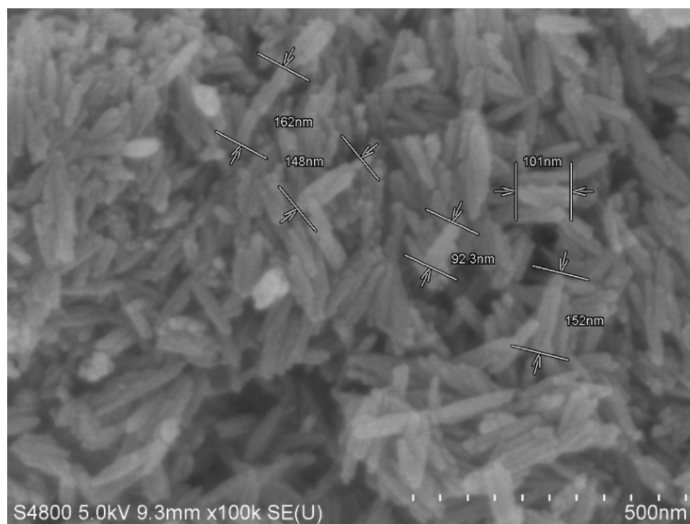


Figure 1. SEM image of Nano-Fe₂O₃.

In contrast, the Nano-Fe₂O₃ is intercepted with a certain thickness of the model to eliminate the error of uneven charge distribution caused by the thinness of the Nano-Fe₂O₃. The detailed molecular composition is shown in Figure 2.

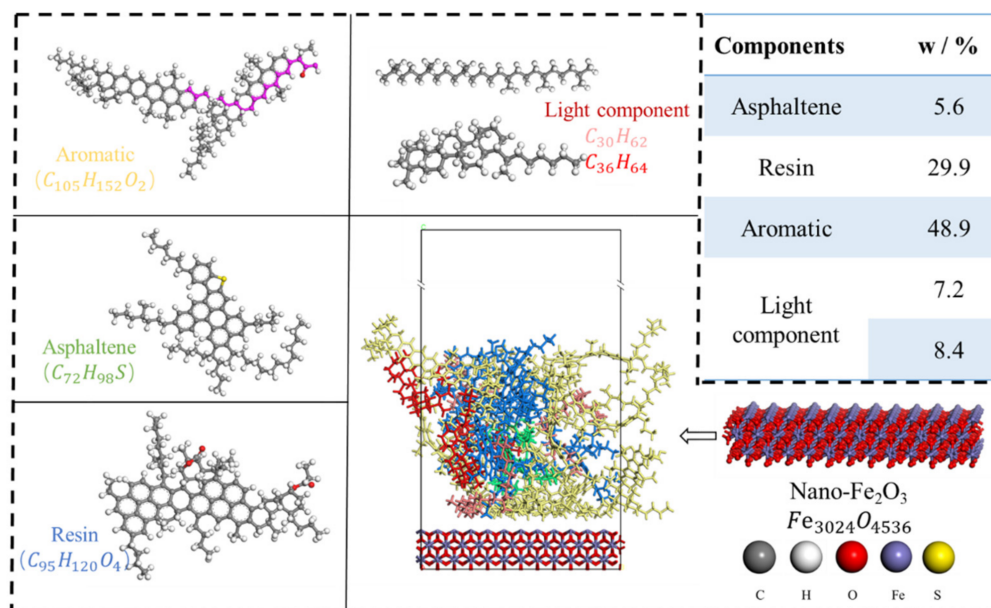


Figure 2. Structural model of asphalt SARA and Nano-Fe₂O₃.

In this paper, the models of asphalt and asphalt/iron oxide nanoparticles were selected for structural optimization, annealing, and radial distribution function (RDF) study based

on molecular dynamics simulations with NPT tethered clone, COMPASS II force field, and Ewald summation method as the computational conditions.

On the constructed asphalt model, the structure is first annealed, and the simulation calculation parameters are generally set to 15 annealing cycles at NPT, 298 K–500 K. After the annealing treatment, the cell length of the constructed asphalt colloidal system model was stabilized between 31.5 and 32 Å, and the density was stabilized between 0.90 and 0.94. The annealed optimized structure was then subjected to molecular dynamics simulations in NPT and NVE for 900 ps to allow the structure to reach a steady state.

3. Results and Discussion

3.1. Evaluation of Basic Physical Properties

From Table 1, it can be seen that the softening point of asphalt composites increases with the increasing amount of Nano-Fe₂O₃ doping, while the ductility and needle penetration are opposite to each other. It is also reflected from the basic physical properties that the incorporation of Nano-Fe₂O₃ can enhance the high-temperature stability of asphalt composites.

Table 1. Effect of different content of Nano-Fe₂O₃ on the properties of asphalt composites.

Nano-Fe ₂ O ₃ (%)	Softening Point (°C)	Penetration Degree (25 °C, 0.1 mm)	Ductility (5 °C, cm)
0	48.6	67.1	73
1	50.2	59.5	65
2	51.2	60.6	52
3	52	60.7	47
4	52.2	56.4	35
5	52.5	54.1	24

With the increasing amount of Nano-Fe₂O₃ doping, the increase of softening point before 1–3% is greater than that of 4–5%. The penetration decreases significantly with the increase of Nano-Fe₂O₃ doping, stabilizes at the content of 1–3%, and then continues to decrease with the increase of Nano-Fe₂O₃ content. The ductility gradually decreases with the increase of Nano-Fe₂O₃ doping and only decreases between 2% and 3% of the content. This phenomenon may occur because the incorporation of Nano-Fe₂O₃ gradually interacts with the stable asphalt colloidal structure. This results in a gradual increase in the softening point of the asphalt and a decrease in the penetration and ductility properties. Overall, the optimal content of Nano-Fe₂O₃ is 2% to 3%.

3.2. Viscosity

Figure 3 shows the effect of different Nano-Fe₂O₃ doping levels on the viscosity of asphalt at different temperatures. From the figure, it can be seen that the viscosity of asphalt increases with the addition of modifier Nano-Fe₂O₃. The viscosity of Nano-Fe₂O₃/asphalt composites has a large increase compared to the matrix asphalt at the doping level of 1–3%. This is because the incorporation of Nano-Fe₂O₃ can effectively interact with the asphalt colloid, such as charge attraction, which leads to the difficulty of the components of Nano-Fe₂O₃/asphalt composites to move with the increase of temperature, which also increases the viscosity of the composites. With the increase of Nano-Fe₂O₃ doping amount up to 4–5%, the viscosity of asphalt large changed more significantly compared to 1–3%. This also indicates that when Nano-Fe₂O₃ reaches large dosing, the factors affecting the viscosity of asphalt are not only the interaction between the modifier and the asphalt colloid but also a large amount of Nano-Fe₂O₃ will exist within the asphalt system, leading to an increase in friction within the Nano-Fe₂O₃/asphalt composite system.

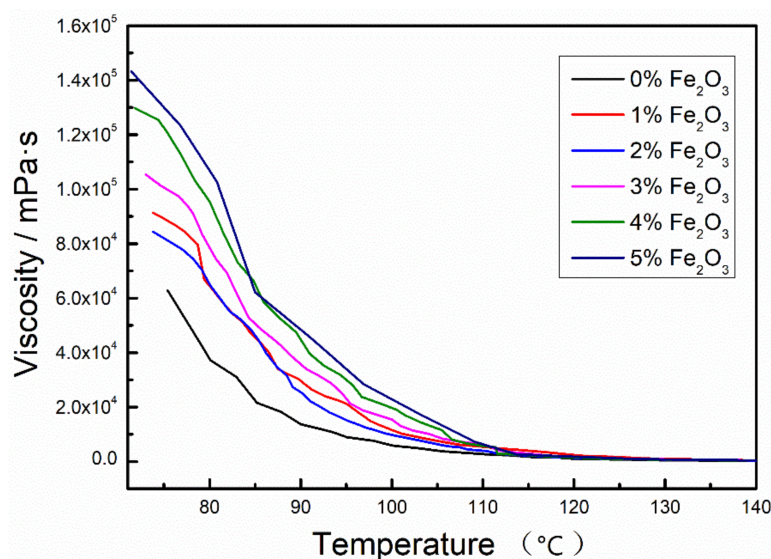


Figure 3. Effect of different Nano-Fe₂O₃ on asphalt viscosity at different temperatures.

3.3. Activation Energy of Viscous Flow

The viscosity η of asphalt at different temperatures T is plotted against $\ln(\eta)$ and $\frac{1}{T}$. The slope of the resulting line is the value of the coefficient of $\frac{1}{T}$, which is the value of $\frac{E_a}{R}$, where R is the universal gas constant ($8.314 \text{ J}\cdot\text{mol}^{-1}\cdot\text{K}^{-1}$), which in turn leads to the E_a of the Nano-Fe₂O₃/asphalt composite.

As shown in Table 2, with the incorporation of Nano-Fe₂O₃, the E_a values of asphalt composites showed a trend of decreasing before increasing. The smallest E_a value was $6.96 \text{ kJ}\cdot\text{mol}^{-1}$ at 1% doping. With the increase of doping amount, the E_a value stabilized at 2–3% doping amount. When Nano-Fe₂O₃ reaches high dosing (4–5%), the E_a values increase again, to $7.93 \text{ kJ}\cdot\text{mol}^{-1}$, $7.78 \text{ kJ}\cdot\text{mol}^{-1}$, and even exceed the $7.16 \text{ kJ}\cdot\text{mol}^{-1}$ of the matrix asphalt. This shows that the matrix asphalt is more flowable and flexible at 1% of Nano-Fe₂O₃, and the asphalt components require less energy to move and have improved temperature sensitivity. The amount of admixture that does not differ much from this is 2% to 3%.

Table 2. Effect of different doping of Nano-Fe₂O₃ on E_a of asphalt composites.

Nano-Fe ₂ O ₃ %	$\ln(\eta) - \frac{1}{T}$	$E_a/\text{kJ}\cdot\text{mol}^{-1}$
0	$y = 897.07x - 0.18$	7.46
1	$y = 837.02x + 0.79$	6.96
2	$y = 912.53x - 0.17$	7.59
3	$y = 894.93x + 0.24$	7.44
4	$y = 954.29x - 0.33$	7.93
5	$y = 936.23x - 0.18$	7.78

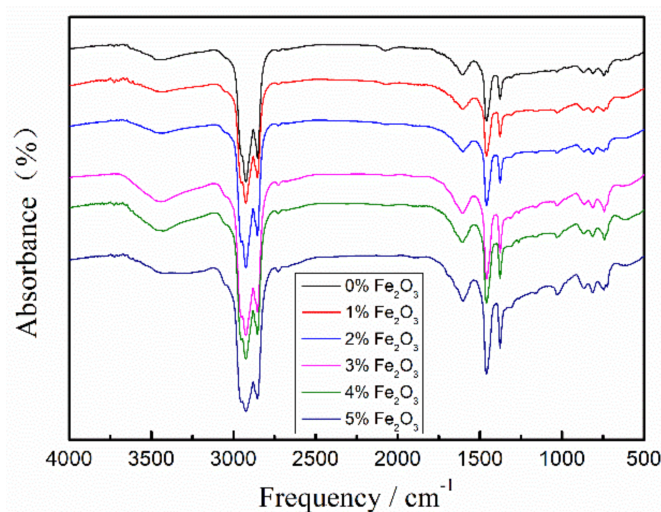
3.4. FTIR Analysis

In this paper, FTIR tests were performed on the Nano-Fe₂O₃/asphalt composite samples, as shown in Table 3, to resolve the main absorption peaks in the Nano-Fe₂O₃/asphalt composite.

As shown in Figure 4, the characteristic peaks of asphalt at 1463 cm^{-1} and 1375 cm^{-1} are caused by the bending vibration of the -CH₂ group in the light component. Additionally, 2920 cm^{-1} and 2852 cm^{-1} are the characteristic peaks of the stretching vibration of the -CH₂ group in the light component. The characteristic peaks of stretching vibrations caused by C = C on the asphalt aromatic ring are at 1600 cm^{-1} and 1480 cm^{-1} . Additionally, the characteristic peak at 710 cm^{-1} is generated by the bending vibration of the alkyl group.

Table 3. Spectral analysis of main absorption peaks in asphalt composites.

Absorption Peaks	Functional Groups
2924 cm^{-1}	Asymmetric stretching vibration of methylene, (C–H)
2853 cm^{-1}	Symmetric stretching vibration of methylene, (C–H)
1601 cm^{-1}	Respiratory vibration of asymmetrically substituted benzene rings
1460 cm^{-1}	Shear vibration of methylene, (–CH ₂ –)
1377 cm^{-1}	Umbrella vibration of methyl, (–CH ₃)
1030 cm^{-1}	Stretching vibration of sulfoxide group, (S=O)
868 cm^{-1}	Stretching vibration of benzene ring
813 cm^{-1}	Stretching vibration of benzene ring
745 cm^{-1}	Bending vibrations of aromatic branched chains
724 cm^{-1}	Co-vibration of methylene chain segment, (CH ₂) _n ($n \geq 4$)

**Figure 4.** FTIR maps of modified asphalt with different Nano-Fe₂O₃ doping.

With the doping of Nano-Fe₂O₃, a relatively weak characteristic peak appears at 1157 cm^{-1} , which is due to the stretching vibration of the C–O bond. The characteristic peaks of the stretching vibration of alkyl sulfoxide (R₂SO) and aryl sulfoxide (S=O) at 1030 cm^{-1} , while the sulfoxide is mainly a dehydrogenation product the components in asphalt.

The incorporation of Nano-Fe₂O₃ did not shift the characteristic peaks of the asphalt, and only the intensity was changed. Together with the changes in the intensity of the characteristic peaks at 1157 cm^{-1} and 1030 cm^{-1} . Therefore, it can be speculated that the interaction between Nano-Fe₂O₃ and the components of asphalt may be mainly physical.

3.5. Microstructure Analysis of AFM

The two-dimensional microscopic morphology in Figure 5 shows that the matrix asphalt has clear “bee structures” with a clear boundary of the structural inclusion phase. This is because the “bee structures” are formed by the co-crystallization of microcrystalline waxes with asphaltenes as the core [7].

When the amount of Nano-Fe₂O₃ doping is 3%, the two-dimensional microstructure shows that the number of “bee structures” characteristic of asphalt decreases, and the “bee structures” become smaller, and most of them gradually. The number of “bee structures” decreases, the “bee structures” become smaller, and most of them are steadily clustered around Nano-Fe₂O₃. Similarly, it can be seen that the surface of asphalt becomes rough due to the incorporation of Nano-Fe₂O₃, but the peaks and valleys of “bee structures” do not disappear but become smaller peaks and valleys. Therefore, we can speculate that the addition of Nano-Fe₂O₃ destroyed the original “bee structures” of the asphalt and formed finer “bee structures”.

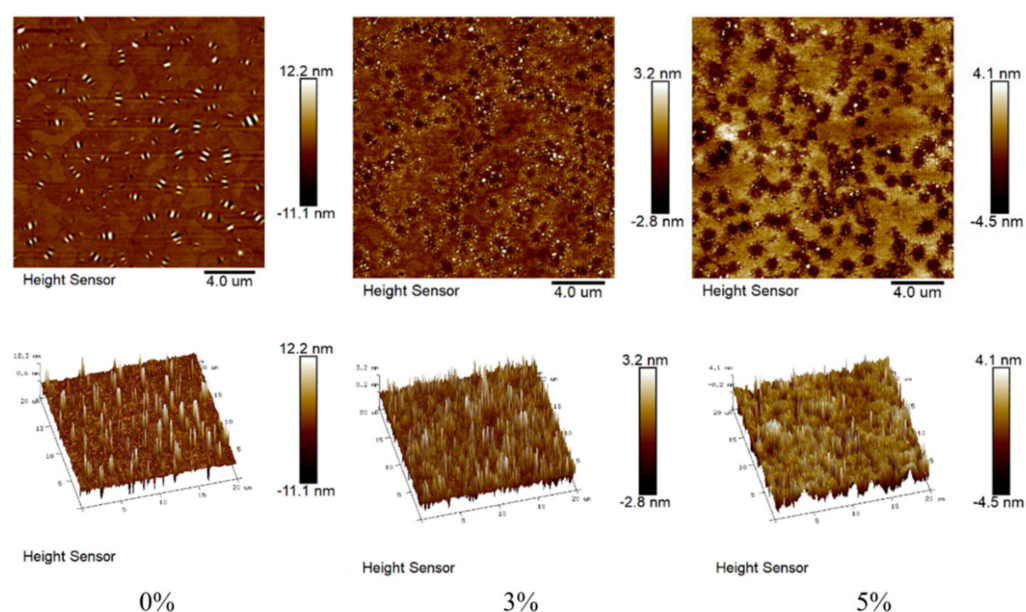


Figure 5. Microscopic characterization of AFM at different doping levels.

The diameter of Nano-Fe₂O₃ increases at 5% doping, probably due to the aggregation of Nano-Fe₂O₃ when it reaches a high doping level. This is probably due to the aggregation of Nano-Fe₂O₃ when it reaches a high doping level, and there are fewer “bee structures” around Nano-Fe₂O₃. From the three-dimensional microstructure, the roughness increased due to the aggregation of Nano-Fe₂O₃, compared to 3%.

This may be because the incorporation of Nano-Fe₂O₃ interacts with the asphalt colloid to reduce the number of microcrystalline waxes used to aggregate around the asphaltene and make it difficult for the asphalt colloid to agglomerate on a large scale. As a result, it is difficult to form obvious and large “bee structures” in the asphalt colloid system, but instead, similar structures like black and white spots are formed.

In terms of colloid theory, the more uniformly dispersed the colloid is, the better its macroscopic properties will be, which also confirms the excellent macroscopic properties of Nano-Fe₂O₃ modified asphalt.

3.6. RDF Analysis Based on Molecular Simulation

As shown in Figure 6, when Nano-Fe₂O₃ was incorporated into the asphalt, the sol-gel structure of the asphalt within the Nano-Fe₂O₃/asphalt composite system was gradually disrupted at temperatures from 208 K to 543 K. With the increasing temperature, the asphaltene shrank from a distance of 23 Å to 19 Å from Nano-Fe₂O₃. When the temperature was raised to 543 K, the distance between the asphaltene and Nano-Fe₂O₃, this suggests that the addition of iron oxide causes the colloidal structure of the asphaltene to move toward the Nano-Fe₂O₃ as the temperature increases and forms the surface interface of the Nano-Fe₂O₃/asphalt composite system. In contrast, the resin keeps aggregating within 10 Å from Nano-Fe₂O₃.

As far as the colloidal structure of asphalt is concerned, the aromatic fraction and resin molecules are mainly clustered around the asphaltene. Most of these three components contain a benzene ring structure, thus creating a “ π - π ” stacking effect. Subsequently, they are distributed among the light components in this state. When Nano-Fe₂O₃ is incorporated into the asphalt as a modifier, with the increase of temperature, asphaltene, aromatic fraction, and resin gradually move to the surface of Nano-Fe₂O₃, forming the interaction between the surface charge of Nano-Fe₂O₃ and the aromatic ring. Additionally, the aromatic fractions gathered around the asphaltene change to gather around Nano-Fe₂O₃. Additionally, when the temperature reaches the high-temperature state (356–543 K), the vibration rate of each component molecule within the asphalt colloidal system is large,

and the asphaltene also gains more molecular vibration kinetic energy because of the increase in temperature, and can even cross the energy barrier between the asphaltene and the molecules adsorbed around it, so that the colloidal structure of asphalt will be destroyed, and thus will gradually approach the surface of Nano-Fe₂O₃. This is also reflected in the AFM diagram; when the iron oxide is incorporated into the asphalt, the “bee structures” will gather around the Nano-Fe₂O₃, and the “bee structures” will become smaller, and the height will also the “bee structures” become smaller and their height decreases.

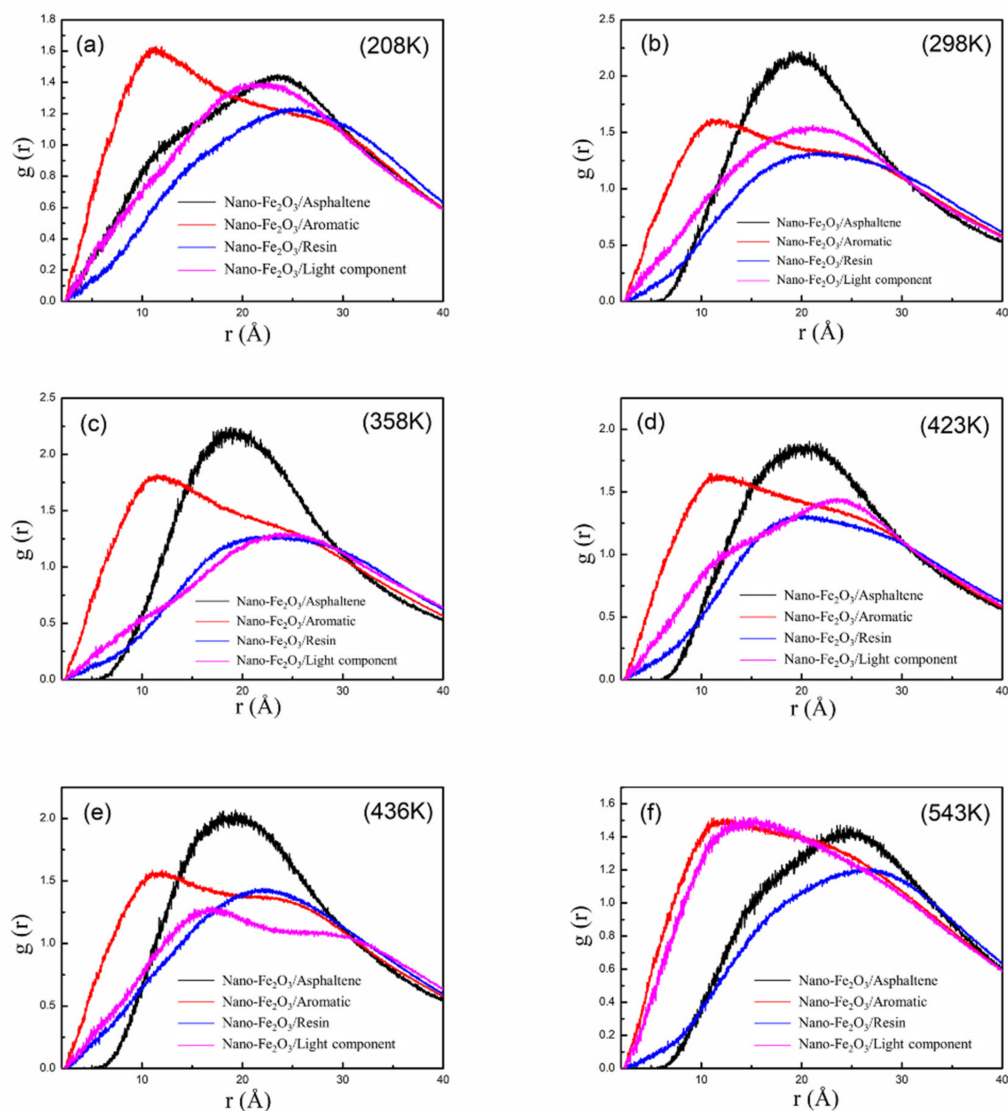


Figure 6. RDF between Nano-Fe₂O₃ and asphalt components in Nano-Fe₂O₃/asphalt composite system. Figures (a–f) are RDF curves at different temperatures.

4. Conclusions

In the Nano-Fe₂O₃/asphalt composites prepared by the high-temperature melting method, the optimal amount of Nano-Fe₂O₃ is 1–3%. Nano-Fe₂O₃ can effectively improve the physical properties of asphalt.

From the AFM diagram, it can be seen that Nano-Fe₂O₃ can be effectively dispersed in the matrix asphalt. The interaction between the asphalt “bee structures” and Nano-Fe₂O₃ is especially obvious at 3% compared with 5%, and it is wrapped around. In this case, the aggregation of the asphalt is effectively prevented, and its molecular movement is hindered. Thus, the physical properties of asphalt composites can be improved. It can be speculated from FTIR that the interaction between Nano-Fe₂O₃ and each component of asphalt may be mainly physical.

When Nano-Fe₂O₃ was incorporated into asphalt, the solvation structure of asphalt within the Nano-Fe₂O₃/asphalt composite system was gradually destroyed at 208 K–543 K. The asphaltene shrank from the distance between structures 23 Å to 19 Å. When the temperature was increased to 543 K, the distance between asphaltene and Nano-Fe₂O₃ increased to 25 with the increase of temperature, the addition of Nano-Fe₂O₃ causes the colloidal structure of asphalt to move toward Nano-Fe₂O₃ and forms the surface interface of the Nano-Fe₂O₃/asphalt composite system.

Author Contributions: Conceptualization, Q.L.; Data curation, Y.H., Y.Z. and Z.X.; Formal analysis, Y.H., Y.Z. and Z.X.; Funding acquisition, Q.L., Y.L., and Q.Z.; Methodology, Y.H., P.L., and Q.Z.; Writing—original draft, Y.H.; Writing—review and editing, Q.L., P.L., and Y.L.; All authors have read and agreed to the published version of the manuscript.

Funding: The authors gratefully acknowledge financial support from the Hunan Innovative Province Construction Special Fund (2019GK508), the Natural Science Foundation of Hunan Province (2020jj4094), the Hunan Provincial Key Laboratory of Flexible Electronic Materials Genome Engineering (2018TP1022), and the Hunan High-tech Industry Science and Technology Innovation Leading Plan (2020GK2012). Qing Zeng would like to acknowledge the support from the Open Research Fund of Hunan Provincial Key Laboratory of Flexible Electronic Materials Genome Engineering (202006).

Institutional Review Board Statement: Not applicable.

Informed Consent Statement: Not applicable.

Data Availability Statement: The data presented in this study are available on request from the corresponding author.

Conflicts of Interest: The authors declare no conflict of interest. The funders had no role in the design of the study; in the collection, analyses, or interpretation of data; in the writing of the manuscript, or in the decision to publish the results.

References

1. Yang, J.; Tighe, S. A Review of Advances of Nanotechnology in Asphalt Mixtures. *Procedia Soc. Behav. Sci.* **2013**, *96*, 1269–1276. [[CrossRef](#)]
2. Liao, G.; Huang, X.; Sang, D.B. Antiultraviolet Aging and Antithermal-Oxygen Aging Tests of Asphalts Adapting to Environment of Tibetan Plateau of China. In Proceedings of the Transportation Research Board 87th Annual Meeting, Washington, DC, USA, 13–17 January 2008.
3. Hao, X.H.; Zhang, A.Q.; Yang, W. Study on the Performance of Nano Calcium Carbonate Modified Asphalt Concrete AC-13. *Adv. Mater. Res.* **2012**, *450–451*, 503–507. [[CrossRef](#)]
4. Steyn, W.J. Applications of Nanotechnology in Road Pavement Engineering. In *Nanotechnology in Civil Infrastructure*; Gopalakrishnan, K., Birgisson, B., Taylor, P., Attoh-Okine, N.O., Eds.; Springer: Berlin/Heidelberg, Germany, 2011; pp. 49–83.
5. Hamedi, G.H.; Nejad, F.M.; Oveisi, K. Estimating the moisture damage of asphalt mixture modified with nano zinc oxide. *Mater. Struct.* **2015**, *49*, 1165–1174. [[CrossRef](#)]
6. Ābele, A.; Merijs-Meri, R.; Bērziņa, R.; Zicāns, J.; Haritonovs, V.; Ivanova, T. Effect of bio-oil on rheological and calorimetric properties of RTFOT aged bituminous compositions. *Int. J. Pavement Res. Technol.* **2021**, *14*, 537–542. [[CrossRef](#)]
7. Wang, P.; Dong, Z.-J.; Tan, Y.; Liu, Z.-Y. Investigating the Interactions of the Saturate, Aromatic, Resin, and Asphaltene Four Fractions in Asphalt Binders by Molecular Simulations. *Energy Fuels* **2015**, *29*, 112–121. [[CrossRef](#)]
8. Hung, A.M.; Mousavi, M.; Fini, E.H. Implication of wax on hindering self-healing processes in bitumen. *Appl. Surf. Sci.* **2020**, *523*, 146449. [[CrossRef](#)]
9. Corbett, L.W. Composition of asphalt based on generic fractionation, using solvent deasphalting, elution-adsorption chromatography, and densimetric characterization. *Anal. Chem.* **2002**, *41*, 576–579. [[CrossRef](#)]
10. Mortazavi, M.; Moulthrop, J.S. *The SHRP Materials Reference Library*; National Academy of Science: Washington, DC, USA, 1993.
11. Claudy, P.; Letoffe, J.; King, G.N.; Brule, B.; Planche, J. Caracterisation Des Bitumes Routiers Par Analyse Calorimetrique Differentielle. *Bull. de Liaison des Lab. des Ponts et Chaussées* **1990**, *165*, 85–92.
12. Pieri, N. Etude Du Vieillissement Simulé et in Situ des Bitumes Routiers par IRTF et Fluorescence UV en Excitation-Émission Synchrones: Détermination des Relations Structures Chimiques-Propriétés Rhéologiques par Analyse en Composantes Principales. Ph.D. Thesis, Aix-Marseille University, Marseille, France, 1994.
13. Callaway, J.; March, N.H. Density Functional Methods: Theory and Applications. *Solid State Phys.* **1984**, *38*, 135–221.
14. Mullins, O.C. Optical Interrogation of Aromatic Moieties in Crude Oils and Asphaltenes. In *Structures and Dynamics of Asphaltenes*; Metzler, J.B., Ed.; Springer: Boston, MA, USA, 1998; pp. 21–77.

15. Scotti, R.; Montanari, L. Molecular structure and intermolecular interaction of asphaltenes by FT-IR, NMR, EPR. In *Structures and Dynamics of Asphaltenes*; Metzler, J.B., Ed.; Springer: Boston, MA, USA, 1998; pp. 79–113.
16. Koots, J.A.; Speight, J.G. Relation of petroleum resins to asphaltenes. *Fuel* **1975**, *54*, 179–184. [[CrossRef](#)]
17. Bergmann, U.; Mullins, O.C.; Cramer, S.P. X-ray Raman spectroscopy of carbon in asphaltene: Light element characterization with bulk sensitivity. *Anal. Chem.* **2000**, *72*, 2609–2612. [[CrossRef](#)] [[PubMed](#)]
18. Michon, L.; Martin, D.; Planche, J.-P.; Hanquet, B. Estimation of average structural parameters of bitumens by ¹³C nuclear magnetic resonance spectroscopy. *Fuel* **1997**, *76*, 9–15. [[CrossRef](#)]
19. Sheremata, J.M.; Gray, M.R.; Dettman, H.D.; McCaffrey, W.C. Quantitative Molecular Representation and Sequential Optimization of Athabasca Asphaltene. *Energy Fuels* **2004**, *18*, 1377–1384. [[CrossRef](#)]
20. Zhao, S.; Kotlyar, L.S.; Sparks, B.D.; Woods, J.R.; Gao, J.; Chung, K.H. Solids contents, properties and molecular structures of asphaltene from different oilsands. *Fuel* **2001**, *80*, 1907–1914. [[CrossRef](#)]
21. Lesueur, D. The colloidal structure of bitumen: Consequences on the rheology and on the mechanisms of bitumen modification. *Adv. Colloid Interface Sci.* **2009**, *145*, 42–82. [[CrossRef](#)] [[PubMed](#)]
22. Mullins, O.C. The Modified Yen Model. *Energy Fuels* **2010**, *24*, 2179–2207. [[CrossRef](#)]